ACS APPLIED NANO MATERIALS

www.acsanm.org Article

Graphene Oxide Composite Membranes for Water Purification

LinSheng Zhu, XiaoXin Guo, YunQiang Chen, Zhou Chen,* YiHong Lan, YuBin Hong,* and WeiGuang Lan*

Cite This: *ACS Appl. Nano Mater.* 2022, 5, 3643−3653 Read Online

ACCESS | Metrics & More | Article Recommendations | Supporting Information

ABSTRACT: Graphene oxide (GO) has attracted remarkable attention as a potential material in the fabrication of next-generation membranes with high water permeability and efficient purification. Herein, an easy and effective means of modifying GO lamellar with a phytic acid (PhA) molecule as both an inserter and a surface modifier was developed to fabricate high-performance GO-based membranes. As a result, the addition of PhA to the GO membrane enhanced hydrophilicity and enlarged the interlamellar spacing. The optimal GP-10 composite membrane displayed a high average pure water flux of 6.31 L m^{-2} h^{-1} bar^{-1} under an ultralow pressure nanofiltration condition, which was about 18.6 times higher than that of 0.34 L m^{-2} h^{-1} bar^{-1} for pure GO membrane. At the same time, it possessed the ability to reject different charged dye molecules with a rejection rate higher than 99.88%. In addition, the composite membrane also showed good structural stability under different pH conditions. This study not only provides a method to simply design GO-based membranes by introducing multifunctional small molecules but also sheds light on using such GO composite membranes in practical water separation applications.

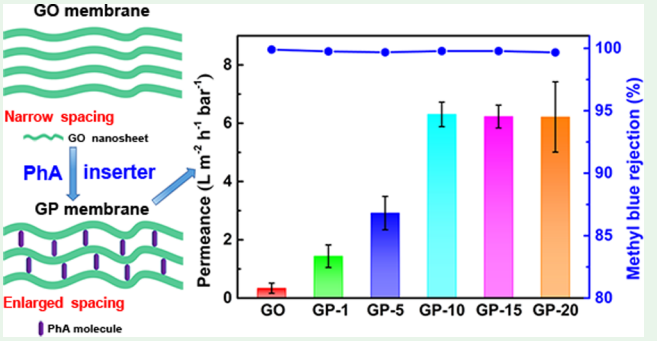

KEYWORDS: *graphene oxide membrane, composite membrane, phytic acid, nanofiltration, low pressure*

1. INTRODUCTION

High-efficiency technologies for water purification are of key significance to solve serious water shortage and water pollution in our modern society.[1−5] As an efficient water treatment technology, membrane filtration has been widely used in wastewater treatment and seawater desalination owing to the advantages of high separation efficiency, low energy consumption, simple operation, and environmental friendliness.[6−11] Nanofiltration (NF) is a type of membrane filtration techniques that can work under relatively low operation pressure but with high permeation flux and rejection rate.[12−15] However, conventional polymer-based NF membranes usually suffer physical aging, poor thermal and chemical resistance, and membrane fouling problems, which hinder their large-scale applications and long periodic running.[16−20] In addition, overcoming the widespread "trade-off" effect between permeability and selectivity is still a major challenge in water treatment-related membrane processes.[21−23] Therefore, smart designing of next-generation advanced NF membranes has received more and more attention in the fields of water purification and molecular separation.

Recently, researchers have mainly focused on searching for new membrane materials to fabricate high-performance NF membranes that can balance the rejection rate and water permeability. Among all available materials, two-dimensional (2D) materials, such as graphene[24] and graphene oxide (GO),[25] owing to their high thermal, chemical, and mechanical stability, atomic thickness, and fast water transport channels, have been considered to be one of the most potential materials for fabricating next-generation advanced NF membranes.[26−30] Because the abundant oxygen-containing functional groups (i.e., −OH, −COOH, epoxy groups) on the edges and the surface of GO enable it to easily disperse in water, the submicrometer-thick GO membrane has promising water transport properties, as a previous study by Geim et al. in 2012 has demonstrated.[31]

However, pure laminar GO membranes usually show low water flux.[32−34] How to improve the water flux of GO-based membranes without sacrificing the rejection rate is crucial for designing the NF membrane devices. Inserting a suitable amount of intercalation materials, including zero-dimensional (0D) materials such as quantum dots,[35] one-dimensional (1D) materials such as Fe_3O_4,[36] SiO_2,[37] TiO_2 nanoparticles,[38,39] oxidized carbon nanotubes (OCNTs),[40−43] 2D materials such

Received: December 13, 2021
Accepted: February 14, 2022
Published: February 23, 2022

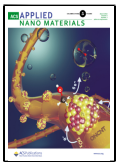

https://doi.org/10.1021/acsanm.1c04322
ACS Appl. Nano Mater. 2022, 5, 3643−3653

as boron nitride (BN)[44] and MoS_2,[45] and three-dimensional (3D) materials such as metal−organic frameworks (MOFs),[46−48] into the interlayer channels to enlarge the interlayer distances has become an effective strategy to enhance water permeance. For example, Jin et al.[36] enlarged the interlayer distances to enhance the water flux by uniformly in situ-growing the Fe_3O_4 nanoparticles on the plane of the GO nanosheet. In 2018, Xu et al.[40] used OCNTs to adjust the interlayer distance of GO and increase the water channel of the membrane through the layer-by-layer self-assembly technique, acquiring a pure water flux of 21.7 L m^{-2} h^{-1} and obtaining a 99.3% rejection rate for methyl blue. Subsequently, they prepared forward osmosis (FO) GOOCNTs-LbL membrane by GO and OCNTs with five bilayers.[42] The results showed that inserting OCNTs in the GO interlayer can increase the layer spacing and thus efficiently improve the water flux. In addition, Jin et al.[46] incorporated 3D nanoporous crystals as intercalators to enlarge the interlamellar spacing, which made the water permeability of the optimized membrane with 14 times enhancements while maintaining a relatively high rejection rate of 98.2% for rhodamine B. However, most of these inserters often cause excessive expansion of the interlayer distances because of their large size and poor interactions between inserters and GO lamellar, which further deteriorates the membrane stability and selectivity.[49,50] The unfavorable swelling effect coming from the excessive inserted agents into the GO nanochannels tends to destroy the interlayer van der Waals forces, which results in an unstable laminar GO structure and thus worsens its performance and selectivity.[51,52] Membrane surface modification with hydrophilic materials is an effective means to further enhance the membrane performance that possesses a high rejection rate and water permeability through the synergistic effect of an inserter and a surface modifier.[53,54] However, fabricating a membrane device with this synergistic effect usually involved a complex process and expensive manufacturing cost. Therefore, it is of great significance to use a simple route that can realize both interlayer cross-linking and surface hydrophilic modification to precisely regulate the membrane structure and thus improve membrane performance and engineer-stabilized nanochannels, which remains to be of high demand.

As a water-soluble natural organic compound, phytic acid (PhA) is readily obtained from grains and beans.[55] It contains six phosphate groups attached symmetrically to a cyclohexanehexol ring. The peculiar molecular structure of PhA makes it possible to serve as an intercalator to modify interlayer distances because the phosphate groups of PhA can easily interact with the oxygen-containing functional groups of GO nanosheets through the formation of multiple hydrogen bonding.[56,57] Meanwhile, the existence of hydroxyl groups endows PhA with good hydrophilicity.[58,59] Consequently, PhA can be used not only as an inserter but also as a surface modifier to modify GO-based membranes.

Here, the uniform dispersion solution of GO and PhA was assembled onto cellulose acetate (CA) membranes via the vacuum filtration method to construct laminar GO/PhA (GP) composite NF membranes. Heat treatment was employed to enhance interactions between GO and PhA, where water molecules were removed and formed a stable C−P bond between GO galleries. Because of the expansion of the interlayer distance and the improvement of hydrophilicity, the pure water flux of the optimally tuned composite membrane is increased 18.6 times from 0.34 L m^{-2} h^{-1} bar^{-1} for the pure GO membrane to 6.31 L m^{-2} h^{-1} bar^{-1} for the GP-10 membrane, while maintaining a high dye rejection rate over 99.88%. Moreover, the optimally tuned composite membrane exhibits good pH tolerance in harsh aqueous solution. This work can arouse more research interests on designing more practical high-performance composite NF membranes for water purification.

2. EXPERIMENTAL SECTION

2.1. Membrane Fabrication. The GO solution was prepared using the modified Hummers' method according to our previous study.[54] In order to fabricate GO and GP composite membranes, 2 mL of GO dispersion (1 mg/mL) was first diluted to 20 mL of deionized (DI) water. Then, different amounts of phytic acid (PhA) solution (0, 0.1, 1, 2, 3, and 4 mL) with a concentration of 10 mg/mL were added and stirred for 2 min. Subsequently, the mixed solution was sonicated for 10 min to make sure a uniform GP suspension with different mass ratios of GO to PhA (1:0, 1:1, 1:5, 1:10, 1:15, and 1:20) was obtained. After that, the uniform GP suspension was assembled onto the supporting CA membranes via the vacuum filtration method. The effective area of the membrane is controlled as 13.08 cm^2. Finally, the composite membrane device was moved into an oven at 90 °C for 0.5 h. The component ratio of the obtained membrane was determined by the mass ratio and was expressed as GP-X, in which X represents the mass ratio of PhA (GO, GP-1, GP-5, GP-10, GP-15, and GP-20, respectively).

2.2. Permeability and Rejection Behavior of the Membranes. The homemade dead-end filtration device was used to measure the pure water flux and dye as well as salt retention, and the effective area is 13.08 cm^2. The specific operation process is as follows: the pure water flux was evaluated using DI water, the rejection behavior was measured using different organic dyes (10 mg/L, including methyl blue (MB), direct red 80 (DR80), Congo red (CR) and rhodamine B (RhB)) and different salt solutions (NaCl, $MgCl_2$, Na_2SO_4, and $MgSO_4$, 2000 ppm). Before the membrane performance test, all membranes were prepressurized for 10 min with an operation pressure of 1 bar. Subsequently, the filtrate was collected and measured every 30 min.

The pure water flux (J) and the rejection rate (R) were calculated as follows:

$$J = \frac{V}{AtP} \tag{1}$$

$$R = \left(1 - \frac{C_p}{C_f}\right) \times 100\% \tag{2}$$

where J, V, A, t, and P represent the pure water permeance (L m^{-2} h^{-1} bar^{-1}), the volume (L) through the filtration membrane, the membrane effective area (m^2), the operation time (h), and the operating pressure condition (bar), respectively. Also, C_P and C_f represent the concentration of the permeate side and the feed side, respectively.

2.3. Membrane Hydrophilicity Influences by the pH Value. To analyze the effect of the pH value on the hydrophilicity of the membrane surface, each membrane was initially soaked in aqueous solution with a pH value of 2 and 12 for 30 min. Then, we took it out and dried it in the oven. The hydrophilicity was characterized using the contact angle test.

2.4. Membrane Reusability Test. The reusability test method of the GP composite membrane was similar to our previous study.[54] In brief, the reusability test was carried out using the filtration-dry-filtration process. After the first filtration, the feed liquid was poured out, and the adsorbed water between layers was pumped out; then, the membrane was made to stand for 30 min at room temperature to complete one cycle. After multiple cycles, the integrity of the GP composite membrane can be judged by the change in the rejection rate, and its strength can be determined at the same time.

https://doi.org/10.1021/acsanm.1c04322
ACS Appl. Nano Mater. 2022, 5, 3643−3653

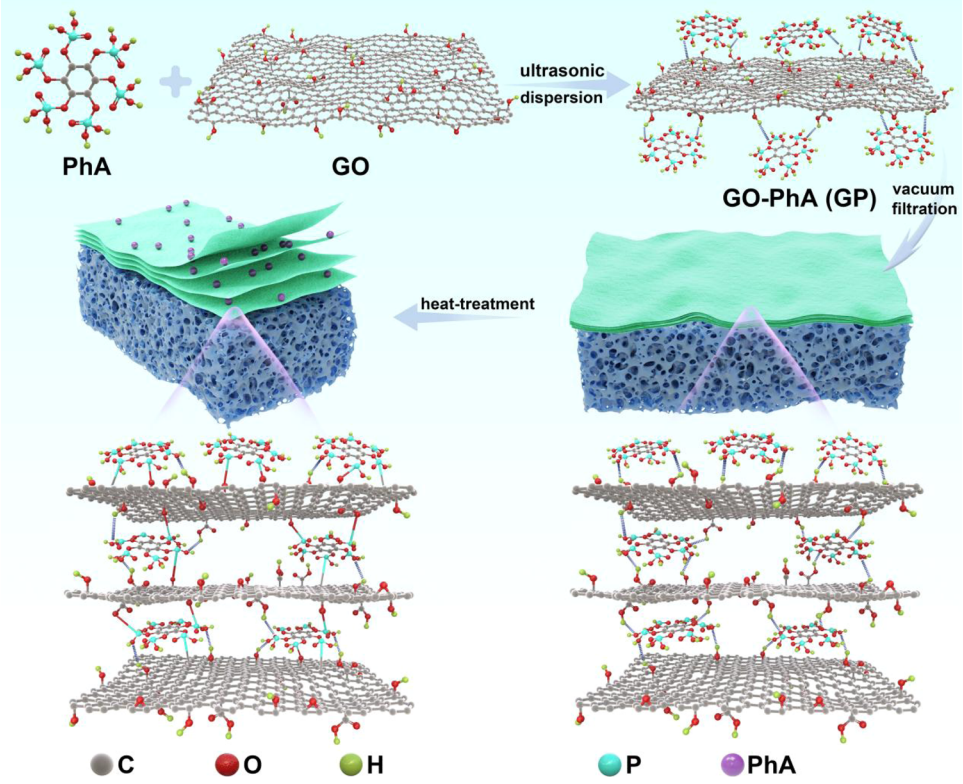

Figure 1. Preparation process of the GP composite membrane.

Detailed materials, membrane characterization methods, and other relevant data are available in the Supporting Information.

3. RESULTS AND DISCUSSION

3.1. Membrane Surface Morphology and Physicochemical Properties. The synthesis process steps of the GP composite membrane are shown in Figure 1. First, PhA was adsorbed on the surface of GO and the formed GP composite through hydrogen bonding under ultrasonic dispersion. Subsequently, the GP solution was assembled on the supporting CA membrane via the vacuum filtration method. To improve the structural strength of the GP membrane, the obtained GP membrane was treated at 90 °C for 30 min, during which the C−P bond was formed between the interlayer of GO nanosheets.

From the digital photographs and SEM images shown in Figures 2a, b and S1, we can see that all the membranes surfaces are intact without any visible defects. Their typical wrinkle morphologies came from the folding effects of GO nanosheets. The cross-sectional morphologies shown in Figures 2c, d and S2 demonstrate that the thickness of GP active layers linearly increases with an increase in the PhA dosage (Figure 2e). The thickness of GP-10 (593.1 nm) is higher than that of GO (417.5 nm), which indicates that PhA molecules have been successfully introduced into the GO interlayer channels and thus will improve the permeation of water through the membrane.

The transmission electron microscopy (TEM) image of GP-10 and the corresponding element mapping are shown in Figures 2f and S3. The GP-10 that links PhA on its surface maintains the nanosheet morphology of GO (Figure S3). Clearly, the C, O, and P elements are uniformly distributed throughout the GP-10 membrane. In addition, the energy-dispersive X-ray spectroscopy (EDS) mapping of GP-10 (Figure S4c and S4d) also exhibits that the phosphorous element is uniformly distributed on the surface and the cross-section of the GP-10 composite membrane, while no phosphorous signals can be detected in pure GO membrane (Figure S4a and S4b). These results further indicate that PhA molecules not only successfully bonded onto the GO surface but also inserted into the interlaminar nanochannels.

The interlayer distances of membranes will determine the separation ability. The pure GO exhibits a narrow X-ray diffraction (XRD) peak at 2θ = 10.82° with an interlayer spacing of 0.818 nm (Figure 2g). For GP membranes, the interlayer distances gradually increase as the content of PhA increases (Figure 2h) as follows: 0.825 nm (GP-1) < 0.836 nm (GP-5) < 0.847 nm (GP-10) < 0.850 nm (GP-15) < 0.852 nm (GP-20). This is because more PhA molecules are inserted into interlaminar channels, resulting in an extended interlayer spacing. It can be expected that an increase in interlayer distances between GO laminates would lead to higher water permeability not only because the interfacial slip effect would reduce[60] but also because the larger interlayer spacing would reduce the transfer resistance and thus become more favorable for the transportation of water molecules.

As shown in Figure S5, pure GO membrane is negatively charged because of the existence of abundant polar functional groups on the GO edges and surfaces.[61] By using PhA molecules with abundant phosphate groups to modify GO, the zeta potential decreases with the increasing PhA content at first, and the GP-10 membrane exhibits the lowest zeta potential of −49.6 mV, which is mainly due to the deprotonation of a large number of phosphoric acid functional groups in PhA molecules introduced into the membrane surface.[62] However, with a further increase in the PhA content,

https://doi.org/10.1021/acsanm.1c04322
ACS Appl. Nano Mater. 2022, 5, 3643−3653

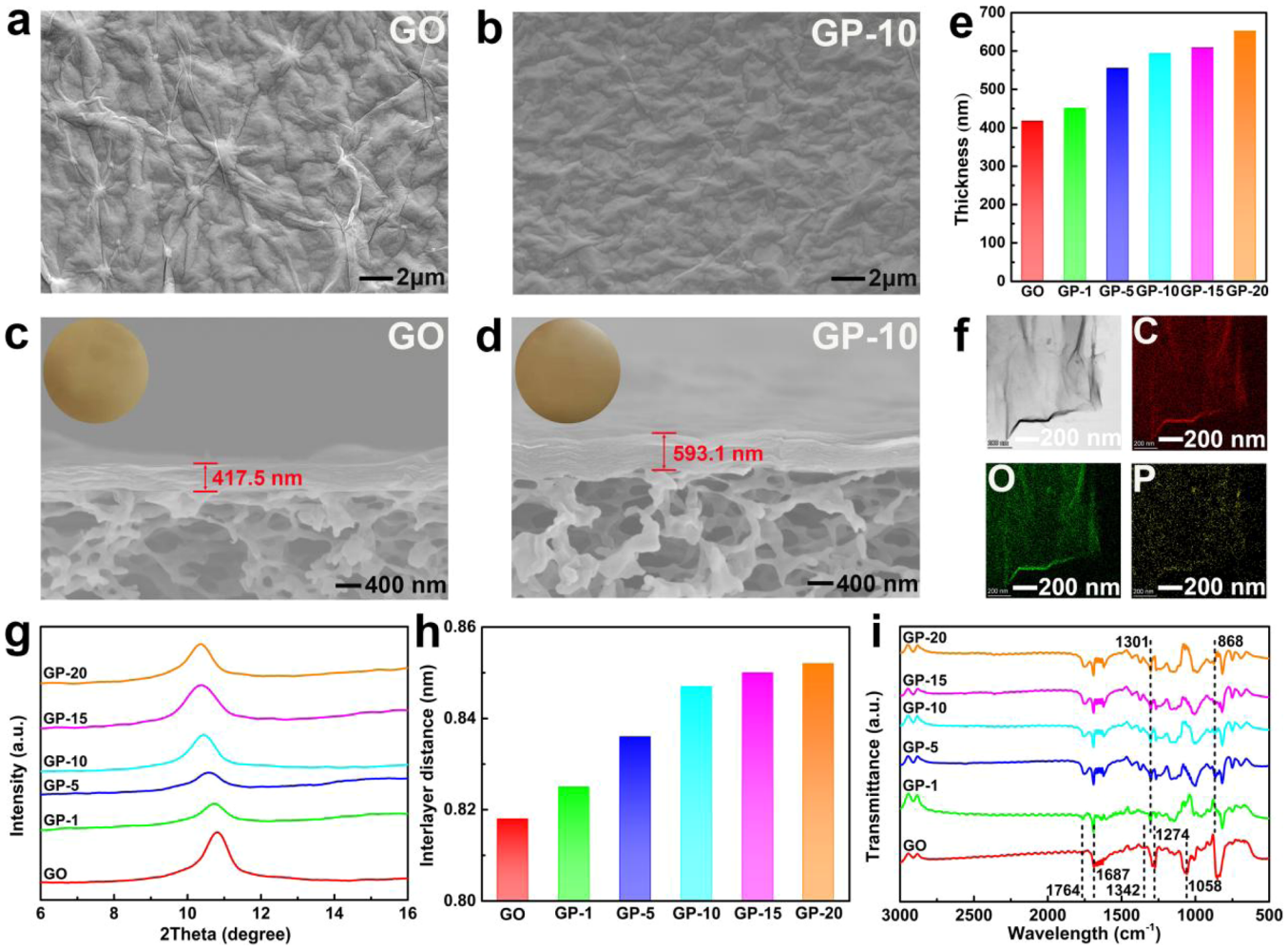

Figure 2. SEM surface images of (a) GO and (b) GP-10 membranes; SEM cross-section images of (c) GO and (d) GP-10 membranes; insets in c and d are the digital photographs of GO and GP-10 membranes; (e) thickness of GO and GP composite membranes; (f) TEM and elemental mapping images of GP-10; (g) XRD patterns of GO and GP composite membranes; (h) interlayer distances of GO and GP composite membranes; (i) FT-IR spectra of GO and GP membranes.

the zeta potential starts to gradually increase again. This is mainly because with the further increase in the PhA content, the pH value of the original solution will further decrease, which would inhibit the deprotonation of the hydroxyl and carboxyl groups on the edge of GO and the phosphate functional groups of PhA molecules, resulting in an increase in the zeta potential.[52,63] Although the change in membrane potential is nonlinear, all the zeta potentials of GO and GP membranes are negative, especially for the GP-10 membrane, which possesses the lowest zeta potential of −49.6 mV. This result further demonstrates the successful modification GO with PhA molecules, and we can expect that the GP-10 that exhibits the lowest zeta potential will have a higher rejection rate for negatively charged dyes and ions owing to the Donnan effect.[64]

3.2. Membrane Surface Chemical Composition. Figure 2i illustrates the Fourier transform infrared (FT-IR) spectra of GO and GP membranes. The spectra of the pure GO membrane show absorption peaks at 1764, 1687, 1342, 1274, and 1058 cm^{-1}, which are attributed to carboxyl C═O, aromatic ring C═C, carboxyl C−O, epoxy C−O, and alkoxy C−O, respectively. This result is consistent with that in a previous report.[65] After being modified by PhA molecules, there are obvious differences in several peaks of GP membranes compared with the GO membrane. For the GP membrane, the disappearance of the vibration peak of carboxyl C−O at 1342 cm^{-1} suggests that the C−P bond is formed. In addition, two new absorption peaks appear at 1301 and 868 cm^{-1}, which are attributed to the stretching vibrations of P═O and P−O−C, respectively.[66] These results further indicate that PhA has been successfully introduced into the GO structure.

The surface chemical compositions of membranes were further characterized by XPS. As revealed in Figure 3a, GO shows two peaks at 285.0 and 533.0 eV, which are attributed to the C 1s and O 1s, respectively. For GP membranes, two new peaks appeared at 134.0 and 192.0 eV, attributing to the P 2s and P 2p derived from the PhA molecule,[67] which indicates that the phosphorous species exist on the GP surface. In addition, Figure 3b exhibits that the C 1s spectrum of GO has three divided peaks at binding energies of 248.8, 287.6, and 289.2 eV, which are assigned to C−C/C═C, C−O, and O−C═O bonds, respectively.[68,69] The O 1s spectrum of GO (Figure 3c) also contains three main peaks at 532.4, 533.2, and 534.1 eV, corresponding to O−C═O, O═C, and O−C.[70]

After the modification of PhA, taking the GP-10 membrane as an example (Figure 3e), the C 1s spectrum is divided into four peaks including C−C/C═C (284.8 eV), C−P (285.7 eV), C−O (287.7 eV), and O−C═O (289.3 eV).[71,72] The O

https://doi.org/10.1021/acsanm.1c04322
ACS Appl. Nano Mater. 2022, 5, 3643−3653

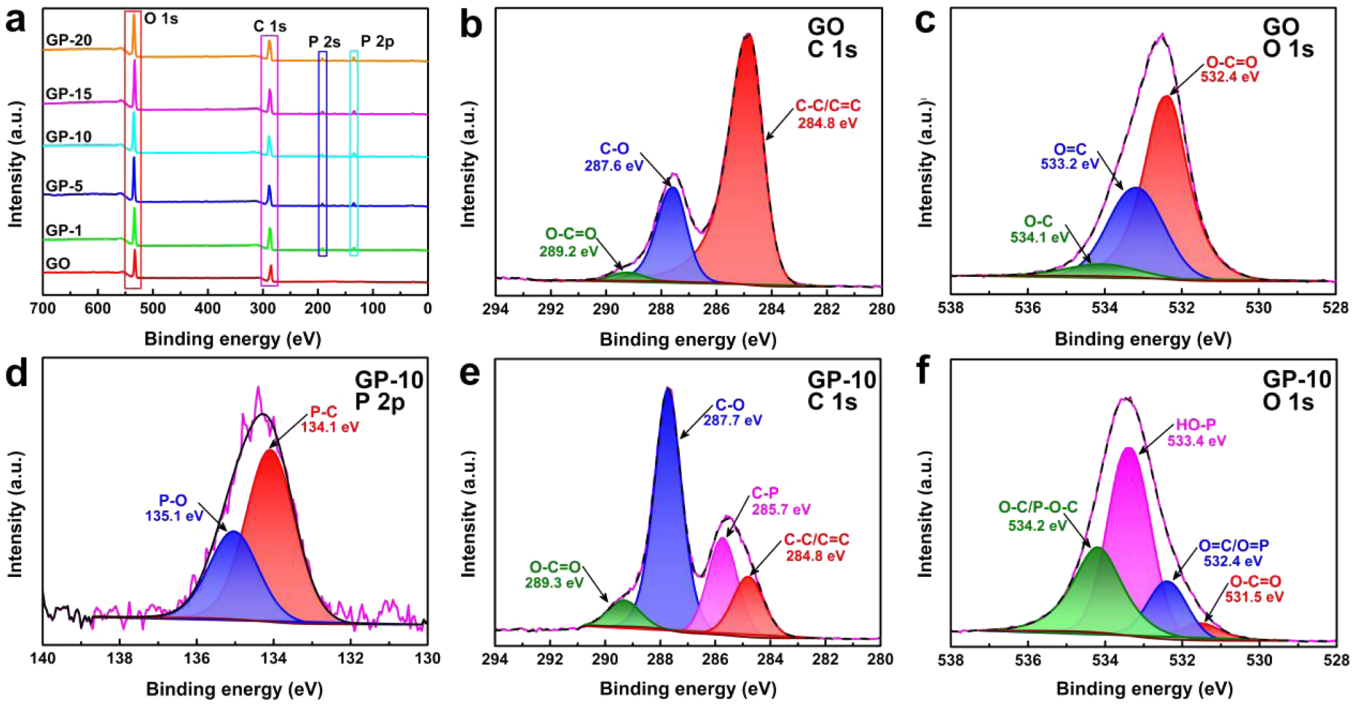

Figure 3. (a) XPS survey spectra of GO and GP composite membranes; high-resolution (b) C 1s and (c) O 1s XPS spectra of the pure GO membrane; high-resolution (d) P 2p, (e) C 1s, and (f) O 1s XPS spectra of the GP-10 membrane.

1s component peaks (Figure 3f) at 531.5, 532.4, 533.4, and 534.2 eV are identified as O−C═O, O═C/O═P, HO−P, and O−C/P−O−C, respectively.[70,73] Meanwhile, the P 2p spectrum with two divided peaks located at 134.1 and 135.1 eV are assigned to P−C and P−O, respectively (Figure 3d).[72,74] The appearance of the new additional peaks (C−P, P═O, and P−OH) verifies the successful decoration of PhA onto the GO surface.[56,57] It should be noted that C−P has been well formed by the dehydration process, and the strong chemical bond between each interlayer will promote the membrane stability during realistic operation.

The element content of the different GO-based membrane surfaces is shown in Table S1. With the increase in the PhA content, the content of P element increases at first and then gradually maintains a relatively stable value. Moreover, the P element can be detected at a depth of 100 nm for GP-10 based on the XPS sputtering depth results (Table S2). These results further demonstrate that PhA not only successfully bonds to the GO surface but also enters the inside of the composite membrane and forms strong chemical bonds between them.

3.3. Membrane Roughness and Hydrophilicity. The surface roughness and hydrophilicity of the membrane play an important role in water permeability. The atomic force microscopy (AFM) surface images and the corresponding 3D topographies of GO and GP composite membranes are shown in Figure 4, and their membrane roughness values are summarized in Table S3. It is clear that the membranes become more smooth after introducing PhA molecules, which agrees well with the surface morphologies investigated by scanning electron microscopy (SEM). The lower roughness of the surface is conducive to the formation of a hydration layer, preventing the adsorption of organic pollutants, thereby improving the durability of the composite membrane according to previous studies.[61,75]

The average contact angels of GO-based membranes are used to measure their hydrophilicity, and the results are shown in Figure 5a. The average contact angles of GO, GP-1, GP-5, GP-10, GP-15, and GP-20 are 60.9°, 47.6°, 40.8°, 29.4°, 29.2°, and 28.1°, respectively. Clearly, the content of hydrophilic PhA molecules has a positive linear correlation with the membrane surface hydrophilicity. The hydrophilic groups on PhA were bonded to the laminar GO surface until a relatively saturated cross-linking value was reached. It can, therefore, be expected that the improved hydrophilicity of GO-based membranes could fasten the diffusion of water molecules and result in high water permeances.[76]

3.4. Membrane Permeability and Separation Performance. As shown in Figure 5b, the pure water flux of GO was only 0.34 L m^{-2} h^{-1} bar^{-1}. Compared to GO, GP composite membranes exhibit improved pure water fluxes because of the increase in the interlayer distances and the improvement of surface hydrophilicity. The pure water flux of GP-1, GP-5, GP-10, GP-15, and GP-20 were 1.44, 2.92, 6.31, 6.23, and 6.22 L m^{-2} h^{-1} bar^{-1}, respectively. Meanwhile, it is worth noting that compared with GP-10, although GP-15 and GP-20 have slightly larger interlayer spacing and higher hydrophilicity, their pure water fluxes are relatively smaller. This is mainly because excessive PhA would block a part of the nanochannels, and the increased thickness of the GP-15 and GP-20 membranes will increase the distance of the mean free path for water molecules, thus resulting in relatively lower pure water fluxes.[77−79]

Subsequently, the cationic MB dye solution was used to carry out the separation performance test on the obtained membranes (Figure 5b), and it can be seen that all the prepared membranes show a high rejection ratio over 99.68%. The relationship between the interlayer spacing and water flux as well as dye rejection for GO and GP membranes is depicted in Figure S6. Clearly, although the increase in the interlayer

https://doi.org/10.1021/acsanm.1c04322
ACS Appl. Nano Mater. 2022, 5, 3643−3653

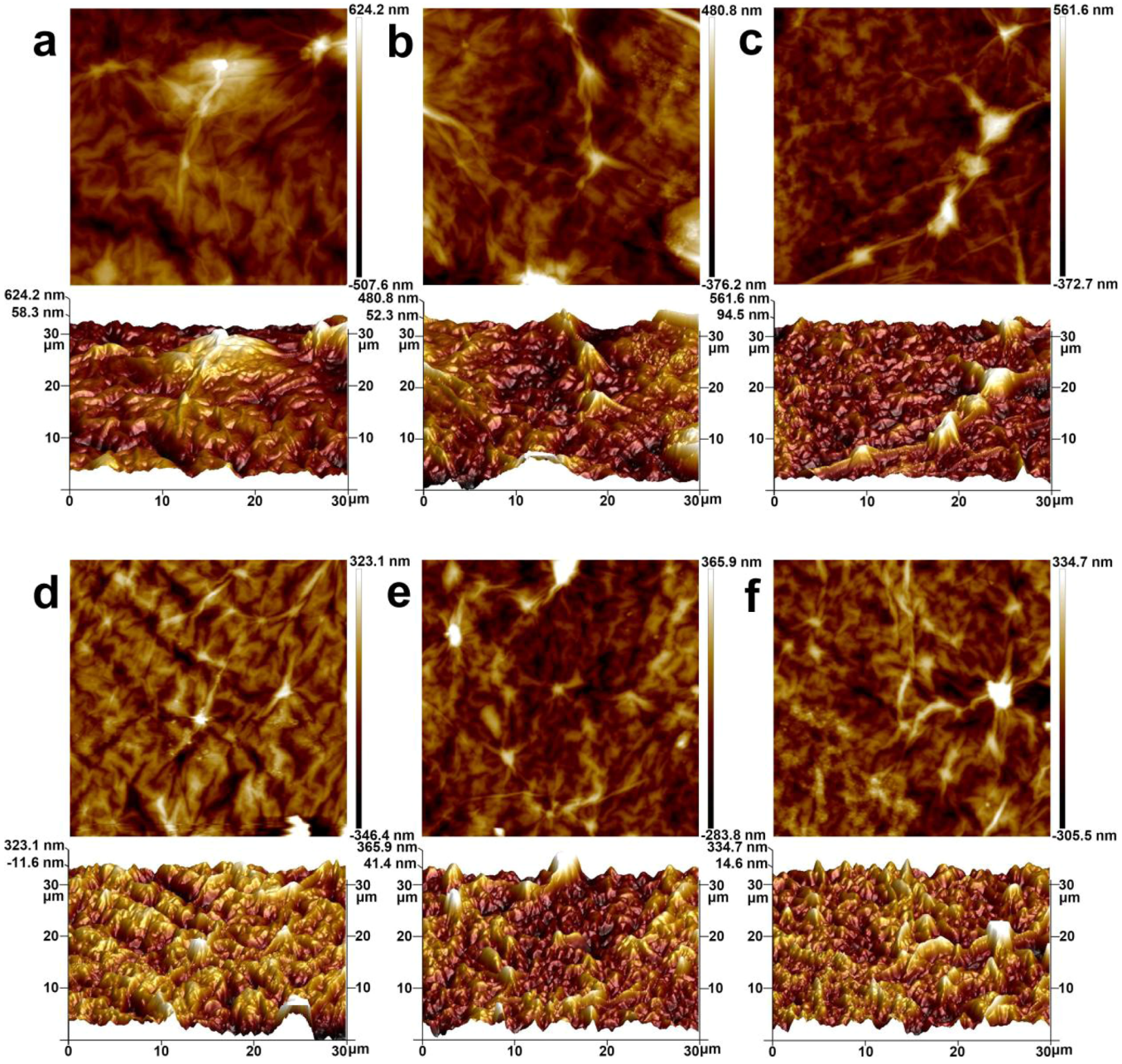

Figure 4. AFM surface images and the corresponding 3D surface morphology images of (a) GO, (b) GP-1, (c) GP-5, (d) GP-10, (e) GP-15, and (f) GP-20 membranes.

spacing makes the rejection rates of GP membranes slightly decrease, the pure water fluxes are effectively increased. When the interlayer spacing increases to about 0.85 nm, the optimal performance of water flux will be shown. Considering the pure water flux of the membranes and minimizing the amount of PhA added, the optimized GP-10 was used as the ideal separation membrane for the following filtration experiments. Four kinds of organic dyes, including positively charged dyes (MB and RhB) and negatively charged dyes (CR and DR80), were used to examine the separation performance of the GP composite membrane. As shown in Figure 5c, the GP-10 composite membrane exhibits a high rejection rate for both positively and negatively charged dyes. The rejection rates of GP-10 for MB, RhB, CR, and DR80 are 99.89, 99.89, 99.94, and 99.91%, respectively.

Then, four kinds of salt ions (2000 ppm Na_2SO_4, $MgSO_4$, $MgCl_2$, and NaCl solutions) were carried out to characterize the salt separation performance of the GP-10 nanofiltration membrane (Figure 5d). As we can see, although the GP-10 composite membrane has high rejection rates for dye solutions, it exhibits poor salt rejection rates for Na_2SO_4, $MgSO_4$, $MgCl_2$, and NaCl with the corresponding rates of 21.08, 15.62, 12.65, and 7.18%. On the basis of this phenomenon, we can expect that the membrane has a potential application prospect in the field of dye desalination and purification.

The effect of the pH of MB solution on the membrane separation performance for the GP-10 membrane was also tested under pH 2, 7, and 12 environments (Figure 5e). The rejection rates of MB are 99.99, 99.89, and 97.14% at pH 2, 7, and 12, respectively. While the rejection rates of DR80 were 99.71, 99.91, and 97.42%. The rejection ratio was all over 97%

https://doi.org/10.1021/acsanm.1c04322
ACS Appl. Nano Mater. 2022, 5, 3643−3653

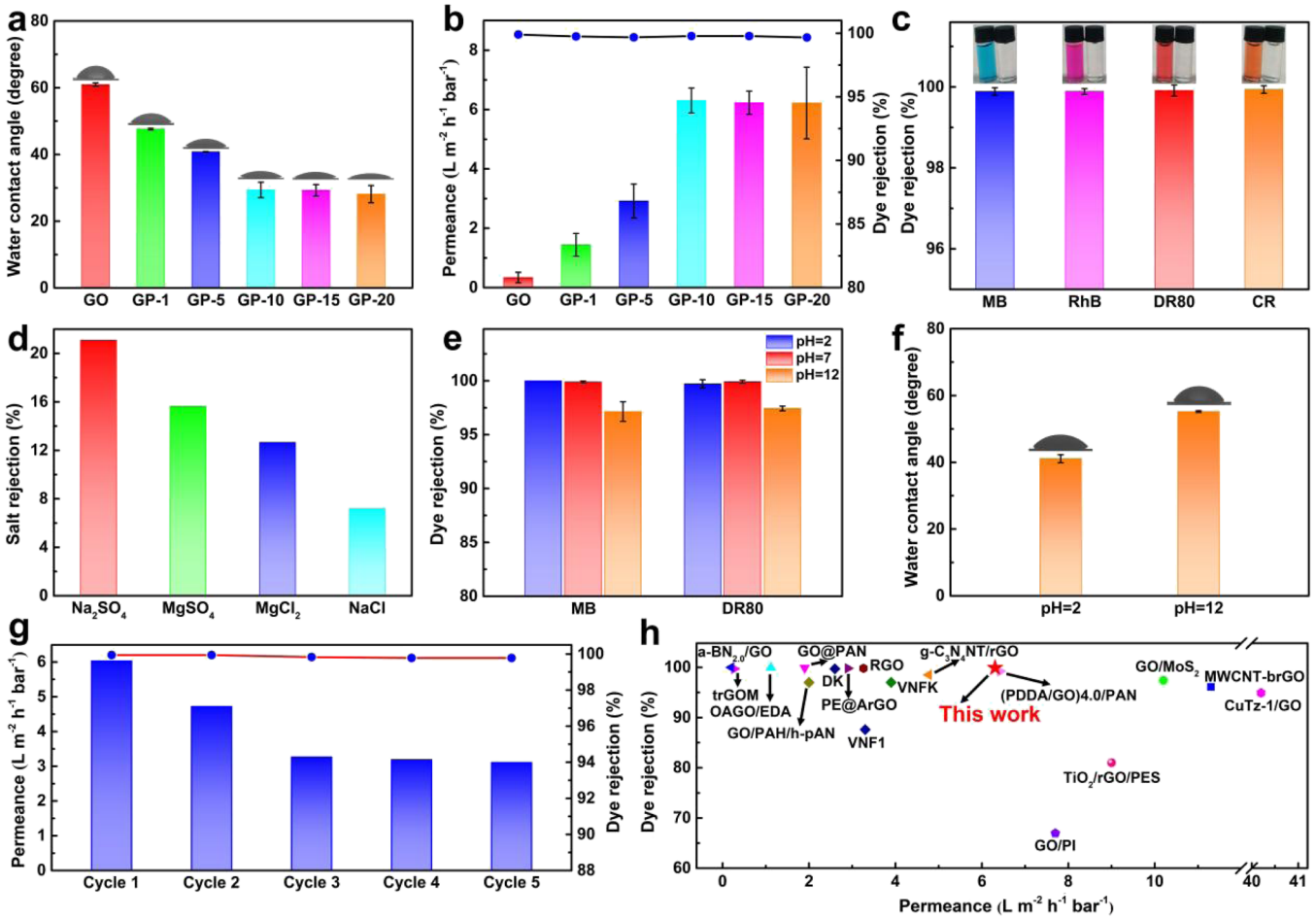

Figure 5. (a) Water contact angles of GO and GP composite membranes; (b) pure water flux and MB rejection of GO and GP composite membranes; (c) dye rejection ratio of GP-10 for MB, RhB, DR80, and CR solution; (d) salt rejection of 2000 ppm salt solution by the GP-10 composite membrane; (e) dye rejection ratio of GP-10 for MB and DR80 at pH 2, 7, and 12; (f) water contact angle of GP-10 in acidic (pH 2) and alkaline (pH 12) environments; (g) reusability of the GP-10 composite membrane for MB dye solution; (h) comparison of the flux and rejection of the GP-10 membrane prepared in our work with the state-of-the-art GO-based membranes and commercial polymeric membranes.

under the experimental pH environments, indicating that the GP-10 membrane has good pH tolerance and can be used in a wide range of pH values.

To further explore the reason why the dye rejection rate of the GP-10 membrane is relatively lower in the alkaline environment, the experiment on the influence of the pH value on the hydrophilicity of the membrane has been performed (Figure 5f). In the alkaline environment, the water contact angle of GP-10 is significantly larger, that is, the surface hydrophilicity is relatively worse. This is mainly because in the strong alkaline environment, PhA molecules on the surface and between the interlayers of the membrane will react with strong alkaline substances such as NaOH to generate sodium phytate and other substances, leading to a significant decrease in the hydrophilic group and thus resulting in reduced hydrophilicity of the membrane surface. At the same time, certain defects would be formed on the surface and between the interlayers of the membrane after the reaction. Therefore, the GP-10 membrane exhibits relatively lower dye rejection in an alkaline environment.

3.5. Durability of the Membrane. The durability of the membrane is an important factor to determine whether the membrane can be used in practical water treatment. Figure 5g exhibits the separation performance of GP-10 for MB solution after 5 cycles. Considering the MB on the membrane surface is not washed out after each cycle, MB was more likely to block the water transport nanochannel with the increasing cycle number. As a result, the MB solution flux was relatively decreased, but the rejection rate still remained at a high rate of over 99.75%. This fact demonstrates that the GP-10 membrane has good mechanical integrity, and thus, the GP-10 membrane can show excellent recycling capability, which enables the GP composite membrane to have a better application prospect in modern industry.

As shown in Figure 5h and in Table S4, we compared our work with previous studies. Various intercalation materials have been used to improve the performance of GO nanofiltration membranes. Although it has been demonstrated that intercalating inserters into the interlayer channels is an effective strategy to enhance water permeance, the balance between water flux and the rejection rate is still supposed to be considered. Clearly, some inserters such as amino-modified boron nitride (a-BN),[44] polyelectrolyte (PE),[80] and graphitic carbon nitride nanotube (g-C_3N_4NT)[81] did not improve flux significantly (0.20 L m^{-2} h^{-1} bar^{-1} to 4.77 L m^{-2} h^{-1} bar^{-1}). Other inserters such as MoS_2,[45] multiwalled carbon nanotubes (MWCNTs),[82] and copper-triazolate MOFs (CuTz-1)[83] can relatively better increase the permeability of GO membranes,

https://doi.org/10.1021/acsanm.1c04322
ACS Appl. Nano Mater. 2022, 5, 3643−3653

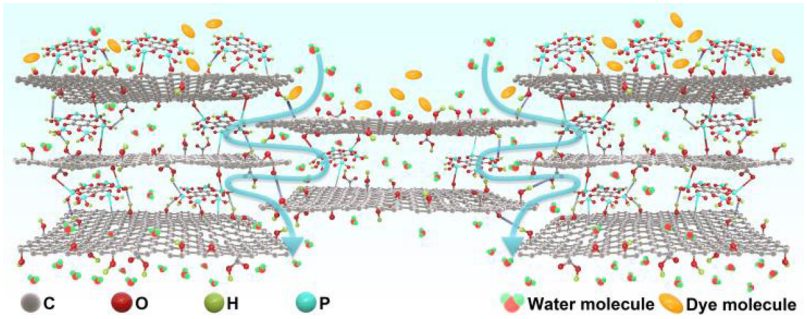

Figure 6. Separation mechanism of the GP NF composite membrane.

while the dye rejection rate would slightly reduce. Moreover, these previous reported membranes usually operated at high pressures (2−20.7 bar), while our GP composite membrane could work efficiently with maintaining excellent dyes rejection and relatively high pure water flux at a much lower pressure (1 bar). Significantly, under the same operating condition, the water flux and the MB rejection of the GP-10 membrane is much higher than those of three commercial membranes (i.e., VNF1, VNFK, and DK), which were studied in our previous work.[54] Therefore, our GP composite membrane shows good potential applications in water treatment.

The mechanism for dye separation by the GP-10 membrane is proposed in Figure 6. To be specific, the high rejection of GP-10 for different charged dyes is mainly attributed to the steric hindrance effect. These dyes with a large size cannot pass through the GP-10 with a smaller interlayer size; therefore, the GP-10 can efficiently intercept these dyes.

4. CONCLUSIONS

In summary, we successfully synthesized high-performance lamellar GP composite membranes through vacuum filtration, in which PhA not only serves as an inserter but also works as a surface modifier to modify GO nanosheets. The improved hydrophilicity and enlarged nanochannels enabled the GP composite membrane to exhibit increased permeability with high rejection for different charge dyes. The optimized membrane GP-10 showed a high water flux of 6.31 L m^{-2} h^{-1} bar^{-1} and good rejection rate of over 99.88% for four kinds of dye solutions. Moreover, the GP-10 membrane can effectively remove anionic dye DR80 and cationic dye MB in a wide range of pH with a rejection rate of over 97%. Importantly, the GP-10 membrane exhibited good tolerance to different pH environments and has good stability for dye rejection after 5 cycles. We believe that our study will provide insights for fabricating high-performance 2D lamellar composite NF membranes by simply introducing multifunctional small molecules.

■ ASSOCIATED CONTENT

Supporting Information

The Supporting Information is available free of charge at https://pubs.acs.org/doi/10.1021/acsanm.1c04322.

Materials, membrane characterization, SEM surface and cross-section images of GP-*X* (*X* = 1, 5, 15, 20) membranes, TEM images, surface and cross-section EDS mappings of GO and GP-10 membranes, zeta potential values of GO and GP membranes, relationship between the interlayer spacing and water flux as well as dye rejection for GO and GP membranes, elemental content by XPS of GO and GP membrane surfaces, elemental content of the GP-10 membrane at different sputtering depths, roughness of GO and GP membranes, comparison of separation performance with the state-of-the-art GO-based membranes and commercial polymeric membranes (PDF)

■ AUTHOR INFORMATION

Corresponding Authors

Zhou Chen − *Xiamen University Center for Membrane Application and Advancement, College of Materials, Xiamen University, Xiamen 361005 Fujian, China;* orcid.org/0000-0001-5398-4654; Email: zhouchen@xmu.edu.cn

YuBin Hong − *Suntar Membrane Technology (Xiamen) Co. Ltd., Xiamen 361022 Fujian, China*; Email: hongyb@suntar.com

WeiGuang Lan − *Xiamen University Center for Membrane Application and Advancement, College of Materials, Xiamen University, Xiamen 361005 Fujian, China; Suntar Membrane Technology (Xiamen) Co. Ltd., Xiamen 361022 Fujian, China;* orcid.org/0000-0002-5556-3113; Email: wglan@xmu.edu.cn

Authors

LinSheng Zhu − *Xiamen University Center for Membrane Application and Advancement, College of Materials, Xiamen University, Xiamen 361005 Fujian, China*

XiaoXin Guo − *Xiamen University Center for Membrane Application and Advancement, College of Materials, Xiamen University, Xiamen 361005 Fujian, China*

YunQiang Chen − *Suntar Membrane Technology (Xiamen) Co. Ltd., Xiamen 361022 Fujian, China*

YiHong Lan − *Suntar Membrane Technology (Xiamen) Co. Ltd., Xiamen 361022 Fujian, China*

Complete contact information is available at: https://pubs.acs.org/10.1021/acsanm.1c04322

Author Contributions

Z.C., Y. Q.C., and L.S.Z. conceived the study and designed the experiments. L.S.Z. and X.X.G. performed the experiments. Z.C and L.S.Z. wrote the article together. W.G.L, Z.C., Y.H.L., and Y.B.H. revised the article. All authors approved the article for publication.

Notes

The authors declare no competing financial interest.

■ ACKNOWLEDGMENTS

This work was funded by Suntar Membrane Technology (Xiamen) Co. Ltd., Xiamen.

REFERENCES

(1) Shannon, M. A.; Bohn, P. W.; Elimelech, M.; Georgiadis, J. G.; Marinas, B. J.; Mayes, A. M. Science and technology for water purification in the coming decades. *Nature* **2008**, *452*, 301−310.

(2) Elimelech, M.; Phillip, W. A. The Future of Seawater Desalination: Energy, Technology, and the Environment. *Science* **2011**, *333*, 712−717.

(3) Sholl, D. S.; Lively, R. P. Seven chemical separations to change the world. *Nature* **2016**, *532*, 435−437.

(4) Greve, P.; Kahil, T.; Mochizuki, J.; Schinko, T.; Satoh, Y.; Burek, P.; Fischer, G.; Tramberend, S.; Burtscher, R.; Langan, S.; Wada, Y. Global assessment of water challenges under uncertainty in water scarcity projections. *Nat. Sustain.* **2018**, *1*, 486−494.

(5) Yadav, S.; Saleem, H.; Ibrar, I.; Naji, O.; Hawari, A. A.; Alanezi, A. A.; Zaidi, S. J.; Altaee, A.; Zhou, J. Recent developments in forward osmosis membranes using carbon-based nanomaterials. *Desalination* **2020**, *482*, No. 114375.

(6) Lee, B.; Baek, Y.; Lee, M.; Jeong, D. H.; Lee, H. H.; Yoon, J.; Kim, Y. H. A carbon nanotube wall membrane for water treatment. *Nat. Commun.* **2015**, *6*, 7109.

(7) Werber, J. R.; Osuji, C. O.; Elimelech, M. Materials for next-generation desalination and water purification membranes. *Nat. Rev. Mater.* **2016**, *1*, 16018.

(8) Park, H. B.; Kamcev, J.; Robeson, L. M.; Elimelech, M.; Freeman, B. D. Maximizing the right stuff: The trade-off between membrane permeability and selectivity. *Science* **2017**, *356*, No. eaab0530.

(9) Wang, X.; Wang, H.; Wang, Y.; Gao, J.; Liu, J.; Zhang, Y. Hydrotalcite/graphene oxide hybrid nanosheets functionalized nanofiltration membrane for desalination. *Desalination* **2019**, *451*, 209−218.

(10) Dharupaneedi, S. P.; Nataraj, S. K.; Nadagouda, M.; Reddy, K. R.; Shukla, S. S.; Aminabhavi, T. M. Membrane-based separation of potential emerging pollutants. *Sep. Purif. Technol.* **2019**, *210*, 850−866.

(11) Nasrollahi, N.; Ghalamchi, L.; Vatanpour, V.; Khataee, A. Photocatalytic-membrane technology: a critical review for membrane fouling mitigation. *J. Ind. Eng. Chem.* **2021**, *93*, 101−116.

(12) Hilal, N.; Al-Zoubi, H.; Darwish, N. A.; Mohammad, A. W.; Abu Arabi, M. A comprehensive review of nanofiltration membranes: Treatment, pretreatment, modelling, and atomic force microscopy. *Desalination* **2004**, *170*, 281−308.

(13) Fritsch, D.; Merten, P.; Heinrich, K.; Lazar, M.; Priske, M. High performance organic solvent nanofiltration membranes: Development and thorough testing of thin film composite membranes made of polymers of intrinsic microporosity (PIMs). *J. Membr. Sci.* **2012**, *401*, 222−231.

(14) Zhu, J.; Uliana, A.; Wang, J.; Yuan, S.; Li, J.; Tian, M.; Simoens, K.; Volodin, A.; Lin, J.; Bernaerts, K.; Zhang, Y.; Van der Bruggen, B. Elevated salt transport of antimicrobial loose nanofiltration membranes enabled by copper nanoparticles via fast bioinspired deposition. *J. Mater. Chem. A* **2016**, *4*, 13211−13222.

(15) Bhol, P.; Yadav, S.; Altaee, A.; Saxena, M.; Misra, P. K.; Samal, A. K. Graphene-Based Membranes for Water and Wastewater Treatment: A Review. *ACS Appl. Nano Mater.* **2021**, *4*, 3274−3293.

(16) Cohen-Tanugi, D.; Grossman, J. C. Nanoporous graphene as a reverse osmosis membrane: Recent insights from theory and simulation. *Desalination* **2015**, *366*, 59−70.

(17) Zhang, Y.; Chung, T.-S. Graphene oxide membranes for nanofiltration. *Curr. Opin. Chem. Eng.* **2017**, *16*, 9−15.

(18) Ye, W.; Liu, H.; Jiang, M.; Lin, J.; Ye, K.; Fang, S.; Xu, Y.; Zhao, S.; Van der Bruggen, B.; He, Z. Sustainable management of landfill leachate concentrate through recovering humic substance as liquid fertilizer by loose nanofiltration. *Water Res.* **2019**, *157*, 555−563.

(19) Levitsky, I.; Tavor, D.; Gitis, V. Microbubbles and organic fouling in flat sheet ultrafiltration membranes. *Sep. Purif. Technol.* **2021**, *268*, No. 118710.

(20) Castelletto, S.; Boretti, A. Advantages, limitations, and future suggestions in studying graphene-based desalination membranes. *RSC Adv.* **2021**, *11*, 7981−8002.

(21) Yan, D.-X.; Pang, H.; Li, B.; Vajtai, R.; Xu, L.; Ren, P.-G.; Wang, J.-H.; Li, Z.-M. Structured Reduced Graphene Oxide/Polymer Composites for Ultra-Efficient Electromagnetic Interference Shielding. *Adv. Funct. Mater.* **2015**, *25*, 559−566.

(22) Zhang, Z.; Xiao, X.; Zhou, Y.; Huang, L.; Wang, Y.; Rong, Q.; Han, Z.; Qu, H.; Zhu, Z.; Xu, S.; Tang, J.; Chen, J. Bioinspired Graphene Oxide Membranes with pH-Responsive Nanochannels for High-Performance Nanofiltration. *ACS Nano* **2021**, *15*, 13178−13187.

(23) Lan, Q.; Feng, C.; Wang, Z.; Li, L.; Wang, Y.; Liu, T. Chemically Laminating Graphene Oxide Nanosheets with Phenolic Nanomeshes for Robust Membranes with Fast Desalination. *Nano Lett.* **2021**, *21*, 8236−8243.

(24) Kuila, T.; Bose, S.; Mishra, A. K.; Khanra, P.; Kim, N. H.; Lee, J. H. Chemical functionalization of graphene and its applications. *Prog. Mater. Sci.* **2012**, *57*, 1061−1105.

(25) Huang, H.; Ying, Y.; Peng, X. Graphene oxide nanosheet: an emerging star material for novel separation membranes. *J. Mater. Chem. A* **2014**, *2*, 13772−13782.

(26) Yang, Q.; Su, Y.; Chi, C.; Cherian, C. T.; Huang, K.; Kravets, V. G.; Wang, F. C.; Zhang, J. C.; Pratt, A.; Grigorenko, A. N.; Guinea, F.; Geim, A. K.; Nair, R. R. Ultrathin graphene-based membrane with precise molecular sieving and ultrafast solvent permeation. *Nat. Mater.* **2017**, *16*, 1198−1202.

(27) Kim, S.; Wang, H.; Lee, Y. M. 2D Nanosheets and Their Composite Membranes for Water, Gas, and Ion Separation. *Angew. Chem., Int. Ed.* **2019**, *58*, 17512−17527.

(28) Zhang, Z.; Huang, L.; Wang, Y.; Yang, K.; Du, Y.; Wang, Y.; Kipper, M. J.; Belfiore, L. A.; Tang, J. Theory and simulation developments of confined mass transport through graphene-based separation membranes. *Phys. Chem. Chem. Phys.* **2020**, *22*, 6032−6057.

(29) Guo, H.; Kong, G.; Yang, G.; Pang, J.; Kang, Z.; Feng, S.; Zhao, L.; Fan, L.; Zhu, L.; Vicente, A.; Peng, P.; Yan, Z.; Sun, D.; Mintova, S. Cross-Linking between Sodalite Nanoparticles and Graphene Oxide in Composite Membranes to Trigger High Gas Permeance, Selectivity, and Stability in Hydrogen Separation. *Angew. Chem., Int. Ed.* **2020**, *59*, 6284−6288.

(30) Kumari, P.; Tripathi, K. M.; Jangir, L. K.; Gupta, R.; Awasthi, K. Recent advances in application of the graphene-based membrane for water purification. *Mater. Today Chem.* **2021**, *22*, No. 100597.

(31) Nair, R. R.; Wu, H. A.; Jayaram, P. N.; Grigorieva, I. V.; Geim, A. K. Unimpeded Permeation of Water Through Helium-Leak-Tight Graphene-Based Membranes. *Science* **2012**, *335*, 442−444.

(32) Liu, Y.; Zhang, F.; Zhu, W.; Su, D.; Sang, Z.; Yan, X.; Li, S.; Liang, J.; Dou, S. X. A multifunctional hierarchical porous SiO_2/GO membrane for high efficiency oil/water separation and dye removal. *Carbon* **2020**, *160*, 88−97.

(33) Ismail, N. H.; Salleh, W. N. W.; Ismail, A. F.; Hasbullah, H.; Yusof, N.; Aziz, F.; Jaafar, J. Hydrophilic polymer-based membrane for oily wastewater treatment: A review. *Sep. Purif. Technol.* **2020**, *233*, No. 116007.

(34) Yan, X.; Cheng, S.; Ma, C.; Li, J.; Wang, G.; Yang, C. D-spacing controllable GO membrane intercalated by sodium tetraborate pentahydrate for dye contamination wastewater treatment. *J. Hazard. Mater.* **2022**, *422*, No. 126939.

(35) Wu, X.; Liu, S.; Cui, X.; Lin, J.; Zhang, H.; Zhang, J.; Wang, J. Manipulating microenvironments of nanochannels in lamellar membranes by quantum dots for highly enhanced nanofiltration performance. *Chem. Eng. Sci.* **2020**, *228*, No. 116001.

(36) Zhang, M.; Guan, K.; Shen, J.; Liu, G.; Fan, Y.; Jin, W. Nanoparticles@rGO Membrane Enabling Highly Enhanced Water Permeability and Structural Stability with Preserved Selectivity. *AIChE J.* **2017**, *63*, 5054−5063.

(37) Deng, H.; Zheng, Q.; Chen, H.; Huang, J.; Yan, H.; Ma, M.; Xia, M.; Pei, K.; Ni, H.; Ye, P. Graphene oxide/silica composite

https://doi.org/10.1021/acsanm.1c04322
ACS Appl. Nano Mater. 2022, 5, 3643−3653

nanofiltration membrane: Adjustment of the channel of water permeation. *Sep. Purif. Technol.* **2022**, *278*, No. 119440.
(38) Chen, L.; Li, N.; Wen, Z.; Zhang, L.; Chen, Q.; Chen, L.; Si, P.; Feng, J.; Li, Y.; Lou, J.; Ci, L. Graphene oxide based membrane intercalated by nanoparticles for high performance nanofiltration application. *Chem. Eng. J.* **2018**, *347*, 12−18.
(39) de Oliveira, C. P. M.; Farah, I. F.; Koch, K.; Drewes, J. E.; Viana, M. M.; Amaral, M. C. S. TiO_2-Graphene oxide nanocomposite membranes: A review. *Sep. Purif. Technol.* **2022**, *280*, No. 119836.
(40) Kang, H.; Shi, J.; Liu, L.; Shan, M.; Xu, Z.; Li, N.; Li, J.; Lv, H.; Qian, X.; Zhao, L. Sandwich morphology and superior dye-removal performances for nanofiltration membranes self-assembled via graphene oxide and carbon nanotubes. *Appl. Surf. Sci.* **2018**, *428*, 990−999.
(41) Liu, L.; Kang, H.; Wang, W.; Xu, Z.; Mai, W.; Li, J.; Lv, H.; Zhao, L.; Qian, X. Layer-by-layer self-assembly of polycation/GO/OCNTs nanofiltration membrane with enhanced stability and flux. *J. Mater. Sci.* **2018**, *53*, 10879−10890.
(42) Kang, H.; Wang, W.; Shi, J.; Xu, Z.; Lv, H.; Qian, X.; Liu, L.; Jing, M.; Li, F.; Niu, J. Interlamination restrictive effect of carbon nanotubes for graphene oxide forward osmosis membrane via layer by layer assembly. *Appl. Surf. Sci.* **2019**, *465*, 1103−1106.
(43) Yu, F.; Shi, H.; Shi, J.; Teng, K.; Xu, Z.; Qian, X. High-performance forward osmosis membrane with ultra-fast water transport channel and ultra-thin polyamide layer. *J. Membr. Sci.* **2020**, *616*, No. 118611.
(44) Lin, H.; Mehra, N.; Li, Y.; Zhu, J. Graphite oxide/boron nitride hybrid membranes: The role of cross-plane laminar bonding for a durable membrane with large water flux and high rejection rate. *J. Membr. Sci.* **2020**, *593*, No. 117401.
(45) Zhang, P.; Gong, J.-L.; Zeng, G.-M.; Song, B.; Cao, W.; Liu, H.-Y.; Huan, S.-Y.; Peng, P. Novel "loose" GO/MoS_2 composites membranes with enhanced permeability for effective salts and dyes rejection at low pressure. *J. Membr. Sci.* **2019**, *574*, 112−123.
(46) Guan, K.; Zhao, D.; Zhang, M.; Shen, J.; Zhou, G.; Liu, G.; Jin, W. 3D nanoporous crystals enabled 2D channels in graphene membrane with enhanced water purification performance. *J. Membr. Sci.* **2017**, *542*, 41−51.
(47) Ying, Y.; Liu, D.; Zhang, W.; Ma, J.; Huang, H.; Yang, Q.; Zhong, C. High-Flux Graphene Oxide Membranes Intercalated by Metal-Organic Framework with Highly Selective Separation of Aqueous Organic Solution. *ACS Appl. Mater. Interfaces* **2017**, *9*, 1710−1718.
(48) Kong, G.; Pang, J.; Tang, Y.; Fan, L.; Sun, H.; Wang, R.; Feng, S.; Feng, Y.; Fan, W.; Kang, W.; Guo, H.; Kang, Z.; Sun, D. Efficient dye nanofiltration of a graphene oxide membrane via combination with a covalent organic framework by hot pressing. *J. Mater. Chem. A* **2019**, *7*, 24301−24310.
(49) Zhang, W.; Shi, M.; Heng, Z.; Zhang, W.; Pan, B. Soft Particles Enable Fast and Selective Water Transport through Graphene Oxide Membranes. *Nano Lett.* **2020**, *20*, 7327−7332.
(50) Guan, J.; You, X.; Shi, B.; Liu, Y.; Yuan, J.; Yang, C.; Pang, X.; Wu, H.; Shen, J.; Fan, C.; Long, M.; Zhang, R.; Jiang, Z. Engineering multi-pathway graphene oxide membranes toward ultrafast water purification. *J. Membr. Sci.* **2021**, *638*, No. 119706.
(51) Sun, P.; Wang, K.; Zhu, H. Recent Developments in Graphene-Based Membranes: Structure, Mass-Transport Mechanism and Potential Applications. *Adv. Mater.* **2016**, *28*, 2287−2310.
(52) Baskoro, F.; Wong, C.-B.; Kumar, S. R.; Chang, C.-W.; Chen, C.-H.; Chen, D. W.; Lue, S. J. Graphene oxide-cation interaction: Inter-layer spacing and zeta potential changes in response to various salt solutions. *J. Membr. Sci.* **2018**, *554*, 253−263.
(53) Chang, R.; Ma, S.; Guo, X.; Xu, J.; Zhong, C.; Huang, R.; Ma, J. Hierarchically Assembled Graphene Oxide Composite Membrane with Self-Healing and High-Efficiency Water Purification Performance. *ACS Appl. Mater. Interfaces* **2019**, *11*, 46251−46260.
(54) Zheng, K.; Li, S.; Chen, Z.; Chen, Y.; Hong, Y.; Lan, W. Highly stable graphene oxide composite nanofiltration membrane. *Nanoscale* **2021**, *13*, 10061−10066.
(55) Yang, L.; Liu, H.; Hu, N. Assembly of electroactive layer-by-layer films of myoglobin and small-molecular phytic acid. *Electrochem. Commun.* **2007**, *9*, 1057−1061.
(56) Zhou, X.; Huang, H.; Zhu, R.; Chen, R.; Sheng, X.; Xie, D.; Mei, Y. Green modification of graphene oxide with phytic acid and its application in anticorrosive water-borne epoxy coatings. *Prog. Org. Coat.* **2020**, *143*, No. 105601.
(57) Chen, G.; Yuan, B.; Wang, Y.; Chen, X.; Huang, C.; Shang, S.; Tao, H.; Liu, J.; Sun, W.; Yang, P.; Shi, G. Nacre-biomimetic graphene oxide paper intercalated by phytic acid and its ultrafast fire-alarm application. *J. Colloid Interface Sci.* **2020**, *578*, 412−421.
(58) Song, X.; Chen, Y.; Rong, M.; Xie, Z.; Zhao, T.; Wang, Y.; Chen, X.; Wolfbeis, O. S. A Phytic Acid Induced Super-Amphiphilic Multifunctional 3D Graphene-Based Foam. *Angew. Chem., Int. Ed.* **2016**, *55*, 3936−3941.
(59) Cai, Y.; Wang, X.; Feng, J.; Zhu, M.; Alsaedi, A.; Hayat, T.; Tan, X. Fully phosphorylated 3D graphene oxide foam for the significantly enhanced U(VI) sequestration. *Environ. Pollut.* **2019**, *249*, 434−442.
(60) Lian, B.; Deng, J.; Leslie, G.; Bustamante, H.; Sahajwalla, V.; Nishina, Y.; Joshi, R. K. Surfactant modified graphene oxide laminates for filtration. *Carbon* **2017**, *116*, 240−245.
(61) Wang, J.; Wang, Y.; Zhu, J.; Zhang, Y.; Liu, J.; Van der Bruggen, B. Construction of TiO_2@graphene oxide incorporated antifouling nanofiltration membrane with elevated filtration performance. *J. Membr. Sci.* **2017**, *533*, 279−288.
(62) Qi, Y.; Tong, T.; Zhao, S.; Zhang, W.; Wang, Z.; Wang, J. Reverse osmosis membrane with simultaneous fouling- and scaling-resistance based on multilayered metal-phytic acid assembly. *J. Membr. Sci.* **2020**, *601*, No. 117888.
(63) Chen, L.; Moon, J.-H.; Ma, X.; Zhang, L.; Chen, Q.; Chen, L.; Peng, R.; Si, P.; Feng, J.; Li, Y.; Lou, J.; Ci, L. High performance graphene oxide nanofiltration membrane prepared by electrospraying for wastewater purification. *Carbon* **2018**, *130*, 487−494.
(64) Zhu, J.; Guo, N.; Zhang, Y.; Yu, L.; Liu, J. Preparation and characterization of negatively charged PES nanofiltration membrane by blending with halloysite nanotubes grated with poly (sodium 4-styrenesulfonate) via surface-initiated ATRP. *J. Membr. Sci.* **2014**, *465*, 91−99.
(65) Pan, F.; Li, Y.; Song, Y.; Wang, M.; Zhang, Y.; Yang, H.; Wang, H.; Jiang, Z. Graphene oxide membranes with fixed interlayer distance via dual crosslinkers for efficient liquid molecular separations. *J. Membr. Sci.* **2020**, *595*, No. 117486.
(66) Jiang, G.; Qiao, J.; Hong, F. Application of phosphoric acid and phytic acid-doped bacterial cellulose as novel proton-conducting membranes to PEMFC. *Int. J. Hydrogen Energy* **2012**, *37*, 9182−9192.
(67) Kim, H. J.; Im, S.; Kim, J. C.; Hong, W. G.; Shin, K.; Jeong, H. Y.; Hong, Y. J. Phytic Acid Doped Polyaniline Nanofibers for Enhanced Aqueous Copper(II) Adsorption Capability. *ACS Sustainable Chem. Eng.* **2017**, *5*, 6654−6664.
(68) Tang, Y. P.; Paul, D. R.; Chung, T. S. Free-standing graphene oxide thin films assembled by a pressurized ultrafiltration method for dehydration of ethanol. *J. Membr. Sci.* **2014**, *458*, 199−208.
(69) Liang, B.; Zhan, W.; Qi, G.; Lin, S.; Nan, Q.; Liu, Y.; Cao, B.; Pan, K. High performance graphene oxide/polyacrylonitrile composite pervaporation membranes for desalination applications. *J. Mater. Chem. A* **2015**, *3*, 5140−5147.
(70) Liu, J.; Yu, Q.; Yu, M.; Li, S.; Zhao, K.; Xue, B.; Zu, H. Silane modification of titanium dioxide-decorated graphene oxide nanocomposite for enhancing anticorrosion performance of epoxy coatings on AA-2024. *J. Alloys Compd.* **2018**, *744*, 728−739.
(71) Yuan, B.; Bao, C.; Qian, X.; Song, L.; Tai, Q.; Liew, K. M.; Hu, Y. Design of artificial nacre-like hybrid films as shielding to mitigate electromagnetic pollution. *Carbon* **2014**, *75*, 178−189.
(72) Wang, J.; Ciucci, F. In-situ synthesis of bimetallic phosphide with carbon tubes as an active electrocatalyst for oxygen evolution reaction. *Appl. Catal., B* **2019**, *254*, 292−299.
(73) Wang, W.; Wang, X.; Pan, Y.; Liew, K. M.; Mohamed, O. A.; Song, L.; Hu, Y. Synthesis of Phosphorylated Graphene Oxide Based

https://doi.org/10.1021/acsanm.1c04322
ACS Appl. Nano Mater. 2022, 5, 3643−3653

Multilayer Coating: Self-Assembly Method and Application for Improving the Fire Safety of Cotton Fabrics. *Ind. Eng. Chem. Res.* **2017**, *56*, 6664−6670.
(74) Lin, D.; Hu, C.; Chen, H.; Qu, J.; Dai, L. Microporous N,P-Codoped Graphitic Nanosheets as an Efficient Electrocatalyst for Oxygen Reduction in Whole pH Range for Energy Conversion and Biosensing Dissolved Oxygen. *Chem. − Eur. J.* **2018**, *24*, 18487−18493.
(75) Safarpour, M.; Khataee, A.; Vatanpour, V. Thin film nanocomposite reverse osmosis membrane modified by reduced graphene oxide/TiO_2 with improved desalination performance. *J. Membr. Sci.* **2015**, *489*, 43−54.
(76) Borges, D. D.; Woellner, C. F.; Autreto, P. A. S.; Galvao, D. S. Insights on the mechanism of water-alcohol separation in multilayer graphene oxide membranes: Entropic versus enthalpic factors. *Carbon* **2018**, *127*, 280−286.
(77) Akbari, A.; Sheath, P.; Martin, S. T.; Shinde, D. B.; Shaibani, M.; Banerjee, P. C.; Tkacz, R.; Bhattacharyya, D.; Majumder, M. Large-area graphene-based nanofiltration membranes by shear alignment of discotic nematic liquid crystals of graphene oxide. *Nat. Commun.* **2016**, *7*, 10891.
(78) Shen, L.; Xiong, S.; Wang, Y. Graphene oxide incorporated thin-film composite membranes for forward osmosis applications. *Chem. Eng. Sci.* **2016**, *143*, 194−205.
(79) Wang, J.; Zhang, P.; Liang, B.; Liu, Y.; Xu, T.; Wang, L.; Cao, B.; Pan, K. Graphene Oxide as an Effective Barrier on a Porous Nanofibrous Membrane for Water Treatment. *ACS Appl. Mater. Interfaces* **2016**, *8*, 6211−6218.
(80) Song, X.; Zambare, R. S.; Qi, S.; Nil, B. S.; Selvaraj, A. P. J.; Tang, C. Y.; Gao, C. Charge-Gated Ion Transport through Polyelectrolyte Intercalated Amine Reduced Graphene Oxide Membranes. *ACS Appl. Mater. Interfaces* **2017**, *9*, 41482−41495.
(81) Wei, Y.; Zhu, Y.; Jiang, Y. Photocatalytic self-cleaning carbon nitride nanotube intercalated reduced graphene oxide membranes for enhanced water purification. *Chem. Eng. J.* **2019**, *356*, 915−925.
(82) Han, Y.; Jiang, Y.; Gao, C. High-Flux Graphene Oxide Nanofiltration Membrane Intercalated by Carbon Nanotubes. *ACS Appl. Mater. Interfaces* **2015**, *7*, 8147−8155.
(83) Zhou, S.; Feng, X.; Zhu, J.; Song, Q.; Yang, G.; Zhang, Y.; Van der Bruggen, B. Self-cleaning loose nanofiltration membranes enabled by photocatalytic Cu-triazolate MOFs for dye/salt separation. *J. Membr. Sci.* **2021**, *623*, No. 119058.

https://doi.org/10.1021/acsanm.1c04322
ACS Appl. Nano Mater. 2022, 5, 3643−3653